PLOS | ONE

RESEARCH ARTICLE

Metabolomic Responses of Guard Cells and Mesophyll Cells to Bicarbonate

Biswapriya B. Misra[1], Evaldo de Armas[2], Zhaohui Tong[3], Sixue Chen[1,4]*

1 Department of Biology, Genetics Institute, Plant Molecular and Cellular Biology Program, University of Florida, Gainesville, FL, 32610, United States of America, **2** Training Institute, Thermo Fisher Scientific, 1400 North point Parkway, Ste 10., West Palm Beach, FL, 33407, United States of America, **3** Department of Agricultural and Biological Engineering, University of Florida, PO Box 110570, Gainesville, FL 32611, United States of America, **4** Interdisciplinary Center for Biotechnology Research, University of Florida, Gainesville, FL 32610, United States of America

* schen@ufl.edu

Citation: Misra BB, de Armas E, Tong Z, Chen S (2015) Metabolomic Responses of Guard Cells and Mesophyll Cells to Bicarbonate. PLoS ONE 10(12): e0144206. doi:10.1371/journal.pone.0144206

Editor: Wagner L. Araujo, Universidade Federal de Vicosa, BRAZIL

Received: September 1, 2015

Accepted: November 13, 2015

Published: December 7, 2015

Data Availability Statement: All relevant data are within the paper and its Supporting Information files.

Funding: This research was supported by National Science Foundation grant MCB-1158000 to SC. The funder had no role in study design, data collection and analysis, decision to publish, or preparation of the manuscript.

Competing Interests: The authors have read the journal's policy and have the following conflict: Co-author Evaldo de Armas was an employee at Thermo Fisher Scientific Inc. when the presented research was performed. This does not alter the authors'

Abstract

Anthropogenic CO_2 presently at 400 ppm is expected to reach 550 ppm in 2050, an increment expected to affect plant growth and productivity. Paired stomatal guard cells (GCs) are the gate-way for water, CO_2, and pathogen, while mesophyll cells (MCs) represent the bulk cell-type of green leaves mainly for photosynthesis. We used the two different cell types, i.e., GCs and MCs from canola *(Brassica napus*) to profile metabolomic changes upon increased CO_2 through supplementation with bicarbonate (HCO_3^-). Two metabolomics platforms enabled quantification of 268 metabolites in a time-course study to reveal short-term responses. The HCO_3^- responsive metabolomes of the cell types differed in their responsiveness. The MCs demonstrated increased amino acids, phenylpropanoids, redox metabolites, auxins and cytokinins, all of which were decreased in GCs in response to HCO_3^-. In addition, the GCs showed differential increases of primary C-metabolites, N-metabolites (e.g., purines and amino acids), and defense-responsive pathways (e.g., alkaloids, phenolics, and flavonoids) as compared to the MCs, indicating differential C/N homeostasis in the cell-types. The metabolomics results provide insights into plant responses and crop productivity under future climatic changes where elevated CO_2 conditions are to take center-stage.

Introduction

Photosynthesis in green plants involves direct CO_2 fixation by the action of ribulose-1,5-bisphosphate carboxylase/oxygenase (RuBisCO) in C3 species and phosphoenolpyruvate carboxylase (PEPCase) in C4 species. With the global climate change scenarios, a rising atmospheric CO_2 concentration [1] can have a significant effect on plant physiology and metabolism and productivity [2]. A steady increase in atmospheric CO_2 levels has been observed over the past 150 years, and this increase is projected to continue [3]. Although the effects of elevated CO_2 on different plants have been studied, e.g., CO_2 improves the photosynthesis of C3 plants, decreases stomatal conductance and photorespiration, and increases energy supply [4],

adherence to all the PLOS ONE policies on sharing data and materials.

Abbreviations: GCs, guard cells; MCs, mesophyll cells; HCO_3^-, bicarbonate; mpi, minutes post-incubation; PEPCase, phosphoenolpyruvate carboxylase; MRM, multiple reaction monitoring; HPLC, high performance liquid chromatography; GC, gas chromatography; LC, liquid chromatography; MS, mass spectrometry.

our knowledge on the global metabolomic changes in different cell-types is extremely limited. While photosynthesis of C3 plants, including major crop species, is stimulated by an increase in the atmospheric CO_2, photosynthetic capacity is often reduced after long-term exposure to elevated CO_2, and there is no information available on short-term plant cellular responses to CO_2 changes at the metabolomic scale. Under elevated CO_2, an initial increase in the rate of carbon fixation was observed in many C3 plants, resulting in the accumulation of main products of photosynthetic carbon assimilation [5].

Omics tools enable systemic view of cellular physiology in a holistic manner to underscore the underlying metabolic networks and regulatory mechanisms. In addition, the use of single-cell types eliminates the 'averaging effect' of metabolomes that occurs in tissue or whole plant studies [6]. For a systemic understanding of cellular functions of GCs, metabolomics approaches have started to provide useful information [7]. Unfortunately, the currently known guard cell metabolome is small, with only about 105 metabolites and a majority of contribution from the reference plant *Arabidopsis thaliana* [8]. The putative roles of these metabolites in stomatal function are summarized in a recent review [9].

Elevated CO_2 increases leaf area and numbers, branching, plant size and biomass, growth rates, C: N ratio and non-structural carbohydrates, in addition to reduced N-compounds such as amino acids and reduced allocation to phenolic compounds [10, 11]. In general, elevated CO_2 may increase agricultural productivity (by increasing starch and sugars etc. by 10–20%) owing to enhanced photosynthesis and water use efficiency, mostly in C_3 crops [12]. Transcriptomic studies conducted in several species such as *A. thaliana* [13, 14], rice (*Oryza sativa*) [15], and *Populus euramericana* [16] have allowed better understanding of the transcriptional basis of plant response to elevated CO_2. Similarly, proteomic changes upon elevated CO_2 were studied in the cash crop halophyte *Aster tripolium* L., which showed that elevated CO_2 enabled an efficient ROS detoxification during salinity stress [17]. In light of the greenhouse effect, how the plants respond to elevated CO_2 in their native growth environment has been the subject of many studies [18]. In *Rumex obtusifolius* L., 1000 ppm CO_2 led to changes in the accumulation of most abundant metabolite oxalate in leaves as revealed by capillary electrophoresis mass spectrometry (CE-MS) analysis [19]. The CO_2 environment plays a huge role in the metabolism of the algae [20]. An early work studied the effect of CO_2 levels in *Chlamydomonas reinhardtii* cells, where 128 metabolites with significant differences between high- and low-CO_2-grown cells were detected, and 82 were identified to include amino acids, lipids, and carbohydrates [21]. Among recent single-cell studies, *C. reinhardtii* proteome, transcriptome and metabolome have been studied under varying CO_2 concentrations [22]. Furthermore, varying CO_2 concentrations induced changes in 25% of the transcriptome in *C. reinhardtii*. Proteomic studies revealed the role of 22 extracellular proteins in *C. reinhardtii*, which are only expressed under low CO_2 conditions [23]. Recently, using GC-ToF-MS, the CO_2 responsiveness of 20 metabolites in GCs was analyzed [24]. How GCs sense the rising CO_2 levels is intriguing as the cellular molecular basis of this response is far from being understood [25].

Atmospheric CO_2 diffuses through the cell wall into the cytosol and dissolves in cell wall or apoplast water to form bicarbonate (HCO_3^-) [26]. The process of dissolving atmospheric CO_2 in water, the subsequent processes of equilibration of dissolved CO_2, HCO_3^- and H_2CO_3, and the diffusion of those dissolved inorganic carbon to cells and the CO_2 fixation sites in chloroplasts are slow physical and chemical processes [23]. An energized conversion of CO_2 to HCO_3^-, however, occurs on the cytosolic side of the thylakoid membrane, i.e., hydration of CO_2 to bicarbonate. Thus, we chose $NaHCO_3$ treatment as a source of CO_2/HCO_3^- to investigate its effect on cellular metabolome. In addition, high HCO_3^--mediated stomatal closure [27] and low HCO_3^--induced stomatal opening [28] are well-known. HCO_3^--induced stomatal movement involves H_2O_2 [29] and NO [27] mediated events. Study of the metabolomes of leaf

cell-types over a time-course may help corroborating the earlier findings, and most importantly reveal novel metabolites involved in the HCO_3^- response. This study on the effect of bicarbonate on the metabolomes of single-cell types in higher plants has not been reported.

Materials and Methods

Plant growth and authentic metabolite standards

Seeds of *B. napus* var. Global obtained from Svalöv Weibull AB (Svalöv, Sweden) were germinated in Metro-Mix 500 potting mixture (The Scotts Co., Marysville, OH, USA), and grown in growth chambers under a photosynthetic flux of 160 μmol photons $m^{-2}s^{-1}$ with a photoperiod of 10 h at 24°C in light and 20°C in dark. Fully expanded leaves from seven week-old plants were used for GCs and MCs enrichment experiments. The metabolite standards were obtained from Sigma-Aldrich (St. Louis, MO, USA). Stock solutions of the 330 compounds were dissolved in appropriate solvents, and prepared as a dilution series in water. The metabolite standards used for the HPLC-MRM-MS library can be found in S1 Table. These solutions were either used immediately or stored in -80°C. Serially diluted stock standard metabolite solutions, ranging in concentration of 0.1–100 pmol μL^{-1} were used to verify the linear response in the mass spectrometer.

Isolation of GCs and MCs for HCO_3^- treatment

Fifteen grams of leaves with main veins removed were blended four times for 15 s each in cold distilled water using a 14-speed Osterizer blender (Oster Inc., Boca Raton, FL). The blended mixture was washed with cold distilled water on a 100 μm Nylon mesh until the flow through was clear of MCs, debris, and plastids. These epidermal peels were then subjected to enzymatic digestion (0.7% Calbiochem cellulysin, 0.025% Macerozyme R10, 0.1% PVP 40, 0.25% BSA) for 50 min in a shaking water bath at 140 rpm in dark. The digest was collected on a nylon mesh (100 μm) and was repeatedly washed using 750 mL of Basic solution (560 mM sorbitol, 5 mM MES, 0.5 mM $CaCl_2$, 0.5 mM $MgCl_2$, 10 μM KH_2PO_4, pH 5.5) to remove broken epidermal (pavement) cells. The enriched GCs were then incubated in stomata opening buffer (50 μM $CaCl_2$, 10 mM KCl, 10 mM MES-KOH, pH 6.2) prepared in Basic solution for an hour in the growth chamber under plant growth conditions. The GC preparations were freshly used.

MCs were isolated as previously described [30] except that the sucrose concentration was 0.7 M. The GCs and MCs were aliquoted in appropriate volumes, and $NaHCO_3$ was added to a final concentration of 1 mM. Cells were incubated for 0, 5, 15, 30, 60, and 120 min on a shaker, and four replicates were generated for each data point. After treatment, the GCs and MCs were immediately frozen in liquid nitrogen and stored in—80°C until metabolite extraction.

Stomatal aperture measurement

Stomatal apertures of the $NaHCO_3$ treated GC preparations were measured using a Zeiss Axiostar Plus microscope (Carl Zeiss Microscopy, Thornwood, NY, USA). Sixty stomata were analyzed in each independent experiment and three such replicate observations were recorded. After incubation, 1 mM $NaHCO_3$ was added to three independent samples where similar volume of H_2O was used as control (mock). At different time points (0, 5, 15, 30, 60, and 120 min.) an aliquot was removed for observation. The results are presented as means ± SE. Data were analyzed using one-way ANOVA using DeviumWeb [31]. A P-value < 0.05 was considered as statistically significant.

Targeted profiling of HCO_3^--responsive metabolomes by HPLC-MRM MS

Targeted metabolite profiling of the untreated and HCO_3^- treated GCs and MCs was performed using HPLC-MRM-MS/MS. Extraction of cellular metabolites was performed as previously described [32]. Extracted metabolites were dissolved in 100 μL H_2O containing three internal standards (33 pmol lidocaine (positive mode), 210 pmol camphor-10-sulfonic acid and 100 pmol adonitol (ribitol) (negative modes) to compensate for retention time shift. The HPLC (Agilent, Santa Clara, CA, USA) used an autosampler (Agilent, Santa Clara, CA, USA) to inject the samples automatically. A C18-reverse phase (Gemini 5μ; 150 × 2.0 mm, Phenomenex, Torrance, CA, USA) analytical column was used with a C18 guard cartridge. The mobile phase consisted of two solvents, i.e., 0.1% formic acid in H_2O (solvent A) and 0.1% formic acid in acetonitrile (solvent B). The HPLC method was run with the following gradient program, i.e., 1:99, v/v, at 0 min; 1:99, v/v, at 0.2 min; 99.5:0.5, v/v at 31 min; 99.5:0.5, v/v at 34 min; 1:99, v/v, at 34.2 min; 1:99 at 60 min at room temperature.

The HPLC was coupled to a hybrid triple quadrupole-ion trap (4000 Q-TRAP, AB Sciex, Foster City, CA, USA) mass spectrometer equipped with a TurboIonSpray (TIS) interface operated in both positive and negative ion modes. The electrospray ionization (ESI) parameters were: curtain gas (CUR) at 30 psi, the ion source (IS) at (+/-) 4500 V, nebulizer gas (GS1) at 50 psi, TIS gas (GS2) at 55 psi and the TIS probe temperature at 350°C. To optimize analyte sensitivity, individual working solutions having the characteristic MRM transition with the optimal declustering potential (DP), collision energy (CE), cell exit potential (CXP) were selected for individual metabolites. Each transition was performed with a 15–40 ms dwell time to get a scan time around 1.2 ms for all the transitions analysed using a method including an enhanced MS scan and an enhanced product ion scan before switching to MRM mode. Essentially, QQQ experiments scans [33] were acquired as MRM experiments where a specific set of MRM transitions were monitored for each run period according to the metabolites eluted within this particular time-frame. We monitored 59 (5.8 min), 40 (9.9 min), 45 (7.9 min), 31 (12.5 min), and 18 (23.8 min) MRM transitions over five periods for the positive ionization mode. For the negative ionization mode, 66 and 11 MRM transitions were recorded for the first and second periods, respectively. Thus, each MRM transition was obtained with a 5-ms dwell time, and the scan mode change was set for 700 ms. The total cycle time was 1–1.5 s for the period, which ensured at least 10 points were obtained for each eluted peak. Data were processed using Analyst^{TM} software version 1.5.1 (AB Sciex, Foster City, CA, USA) while peak areas were integrated using the IntelliQuan algorithm of the MuliQuant^{TM} software version 2.1 (AB Sciex, Foster City, CA, USA). The optimized parameters used for MRM experiments for each standard metabolite included in HPLC-MRM-MS/MS library are provided (S1 Table). Multiple blank solutions were prepared by adding only extraction solvent (buffer) and distilled water, respectively, whereas pooled samples were used as quality control (QC) runs for monitoring the chromatography and mass spectrometer conditions.

Profiling of HCO_3^--responsive metabolomes by GC-MS

Gas chromatography-mass spectrometry was performed as described [34]. Metabolite extracts were dried under vacuum without heating, and were then sequentially derivatized with methoxyamine hydrochloride (MeOX) and *N*-methyl-*N*-trimethylsilyl-trifluoroacetamide (MSTFA) [34]. Derivatization was carried out by adding 50 μL of MeOX (20 mg mL^{-1}) in pyridine and shaking at 30°C for 90 min. followed by trimethylsilylation for 30 min at 37°C by addition of 100 μL MSTFA. One microliter of the derivatized sample was injected in splitless mode into a GC-MS system consisting of an autosampler and a TSQ8000 Triple Quadrupole

(Thermo Scientific Inc., San Jose, CA, USA) or a 5977A Series GC/MSD (Agilent Technologies, Santa Clara, CA, USA) equipped with an electron impact (EI) ionization source. Injection of the sample was performed at 250°C with helium as a carrier gas and flow set to 2 mL min^{-1}. GC was performed using a TR-5MS or HP-5MS capillary column (30 m × 0.25 mm × 0.25 μm). The temperature program started isothermal at 70°C for 1 min followed by a 6°C min^{-1} ramp to 300°C and a final 11 min hold at 300°C. The system was then temperature-equilibrated at 70°C for 5 min before the next injection. Mass spectra were collected at 20 scans/s with a range of *m/z* 40–600. The transfer line and the ion source temperatures were set to 250°C. A standard alkane mixture (C_8-C_{40}) was injected at the beginning and end of the analysis for tentative identification and monitoring shifts in retention indices (RI).

Processing of raw mass spectrometry data

GC-MS data analysis. The GC-MS data were aligned and processed as described [35]. Aligned data were deconvoluted using Automated Mass Spectral Deconvolution and Identification System (AMDIS, National Institute of Standards and Technology, USA). The filtered raw GC-MS data comprised of data from four biological replicates and 73 curated analytes. Peak areas of the mass fragments (*m/z*) were normalized against the internal standard (adonitol). Metabolites were identified by comparing fragmentation patterns available in the MSRI spectral libraries of Golm Metabolome Database available from Max-Planck-Institute for Plant Physiology, Golm, Germany (http://csbdb.mpimp-golm.mpg.de/csbdb/gmd/gmd.html) by matching the mass spectra and RI [36]. Additional peak identification was confirmed by comparing against the NIST Mass Spectral Reference Library (NIST08/2008, National Institute of Standards and Technology, USA). Peak finding and quantification of selective ion traces were accomplished using AMDIS software. As a rule, if a compound had an AMDIS match factor of >60% and a probability score >20% as well as a matching RI to a known compound it was considered "probable". Peak areas were normalized by dividing each peak area value by the area of the internal standard for a specific sample, and were further median normalized. Individual metabolite quantification data were assembled into a joint data set which included those measured by the targeted HPLC-MRM-MS.

Statistical analysis. Statistical analyses were performed using the statistical software R (Version 2.9.1, R Development Core Team 2007, http://www.R-project.org) [37]. When data were not normally distributed, normal transformations of continuous variables were attempted using DeviumWeb [31]. Normalized, transformed, imputed, outlier removed, and scaled peak area representative of relative metabolite amounts are presented in tables and figures. Values reported in all tables and text are presented as means, and differences were always considered significant when $P < 0.05$. **Univariate analysis:** Creation of the heat map and Student's *t*-test (ANOVA-background) were performed using Microsoft Excel (Microsoft Corporation, Seattle, WA, USA). For heat maps, the data were normalized using z-scores of the intensity counts for each of the metabolites under the peak areas. The *t*-test was performed two-sided with equal or unequal variance, where the P-values were adjusted by Benjamini-Hochberg correction (BH) [38]. ANOVA was used to test for differences of the final model's selected variables between cell-types with HCO_3^--and control (H_2O) treatment. The probability level for the test statistics was set at $\alpha = 0.05$ and was adjusted for multiple hypotheses testing using BH to allow for a maximum 5% probability ($q = 0.05$) in false positive detection. Hierarchical clustering analysis (HCA) using average linkage clustering was performed on Euclidean distances using PermutMatrix [39]. Volcano plots were constructed using Multiplot version 2 available at GenePattern server [40]. **Multivariate analysis:** Principal components analysis (PCA) was performed at DeviumWeb [31], where output consisted of score plots to visualize the contrast between

different samples and loading plots to explain the cluster separation. The data file was scaled with unit variance without any transformation. O-PLS-DA was used to highlight differences between control and HCO_3^--treated metabolic phenotypes, for time-points and cell-types used in the study. Orthogonal partial least-squares discriminant analysis (O-PLS-DA) model was developed and plotted to explore the variation in metabolites, visualize their discrimination power, and determine their importance in predicting cellular response to treatments and time-points.

Pathway enrichment and clustering analysis

Pathway enrichment was performed at Metaboanalyst (www.Metaboanalyst.ca) [41]. Briefly, increased or decreased metabolites that changed by 1.2 folds (increase) and 0.8 fold (decrease) were used as cutoffs across the biological replicates, treatments, and time-points indicating that the specific pathway enrichment levels would not be expected by random chance. In addition, pathway mapping were done using MBRole (http://csbg.cnb.csic.es/mbrole/), MSEA (http://www.msea.ca/MSEA/) and MetPA (http://metpa.metabolomics.ca/MetPA/) were used for additional over-representation analyses. For ID conversions, the Chemical Translation Service (CTS: http://cts.fiehnlab.ucdavis.edu/conversion/batch) was used to convert the common chemical names into their KEGG, HMDB, and InChiKeys (S1 Table). For clustering of time-course patterns, Short Time series Expression Miner (STEM) was used as a Java implementation with a graphical user interface (http://www.cs.cmu.edu/~jernst/st/) [42].

Results

HCO_3^--mediated stomatal movement in *B. napus*

To test the effect of HCO_3^- on *B. napus* stomatal movement, we administered $NaHCO_3$ at concentrations of 0 (control) and 1 mM (treatment) to the isolated stomatal GCs (Fig 1). The results clearly showed that 1 mM HCO_3^- was effective in significant reduction of stomatal aperture beyond 30 min post incubation (mpi) as compared to the control. In comparison, MCs did not show any recordable phenotypic changes under 1 mM HCO_3^- treatment.

Cataloging the MC and GC metabolomes and their responses to HCO_3^- treatment

Using a two-pronged approach of targeted HPLC-MRM-MS and GC-MS, we detected and quantified a total of 268 metabolites in MCs and GCs at various time-points across four biological replicates (S1 and S2 Tables). These metabolites covered various metabolic pathways such as purine, pyrimidine, amino acid, central carbon, TCA, sugar, glyoxylate, phenylpropanoid, and flavonoid metabolism that were spread over the KEGG metabolic map (S1 Fig). The root mean square deviation (RSD) analyses of the data indicated that about 95% showed 10–20% RSD for each of the cell types, while the rest 5% were distributed between 30–40%.

The HCO_3^- treated MC and GC metabolomes showed quantitative variations during the time-course experiment. The shared metabolites in MCs and GCs showed differential levels of changes (fold change cut-offs of < 0.8 and >1.2, at $P < 0.05$) (S3 and S4 Tables). To understand the detailed information arising from the multivariate analyses and to identify metabolite features that are significantly different between each time point of HCO_3^- treatment, univariate statistical analyses including t-tests, fold change (FC) and volcano plots were conducted. The Volcano plots revealed that throughout the entire time-course, mostly the amino acids showed significant increases in MCs (except for 30 mpi), with increased accumulation of phenylpropanoids at 30 mpi and 60 mpi only (S2 Fig). In contrast, in the early time-points of 5, 15 and 30

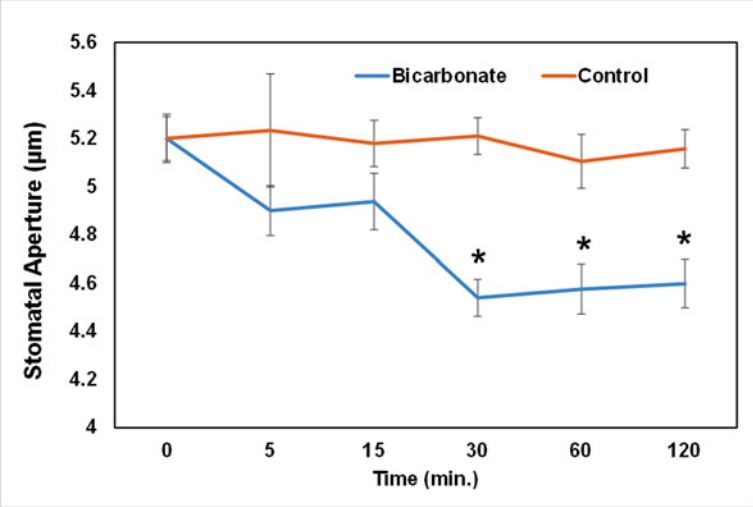

Fig 1. Stomatal movement in response to 1 mM HCO_3^- added at time 0 min. Data were obtained from 60 stomata in three independent experiments and presented as means ± SE. The asterisks indicate significantly different mean values at P <0.05.

doi:10.1371/journal.pone.0144206.g001

mpi sugars, sugar phosphates, and organic acids showed significant increases in GCs, while decreases of phenylpropanoids and flavonoids were noted (S3 Fig). In addition, reduced levels of some phytohormones at 60 mpi and increases in some flavonoids and phenylpropanoids at 120 mpi were also noted in the GCs.

Between subject-ANOVA analysis using the three factors as cell-type (MC vs. GC), treatment (control vs. HCO_3^-), and time-course (0–120 mpi) indicated that HCO_3^- treatment showed tremendous effect on purine, pyrimidine, flavone and flavonol, and alkaloid metabolism whereas time-effect was prominent in pyrimidine, arginine, and glyoxylate metabolism in GCs (S5 Table). In contrast, the MCs showed significant enrichment of taurine, valine, glutathione, amino acid, glycine, serine and nitrogen metabolism after the HCO_3^- treatment, whereas time-effect showed enrichment of amino acid, fructose, and aminosugar metabolism (S5 Table). Although in GCs time and treatment showed interaction for metabolites enriched in pyrimidine, arginine, proline, and glyoxylate metabolism, such interactions were missing in MCs.

Temporal metabolomic changes in HCO_3^- treated MCs and GCs

Many metabolites are shared between MCs and GCs at different time points. Six and 13 metabolites (enriched in phenylalanine and vitamin B6 metabolism) were common to all the five time-points for MCs and GCs, respectively (S6 Table). In addition, hydroxyflavone, vanillin and hexadecanoic acid were common at 5 mpi, 60 mpi and 120 mpi, respectively. Other significantly changed metabolites common between MCs and GCs include 1-ACC, 6-furfurylaminopurine, allantoin, creatine, GSH (reduced glutathione), L-homomethionine, indole butyric acid, and lactose. There were 52 metabolites common to the two cell-types that changed significantly at least in one cell-type at one time point (S7 Table). Hierarchical clustering analysis (HCA) was performed to classify metabolites and time-course profiles into clusters of different trends of changes (Fig 2). Interestingly, we found that these time-resolved metabotypes were discriminated into five distinct clusters. In the first cluster, galactose, glyoxylate, TCA cycle, and pyruvate metabolites were grouped, where increases were mostly in the MCs. In the second cluster purine, arginine, proline, glutathione, and flavonoid metabolites showed large increases

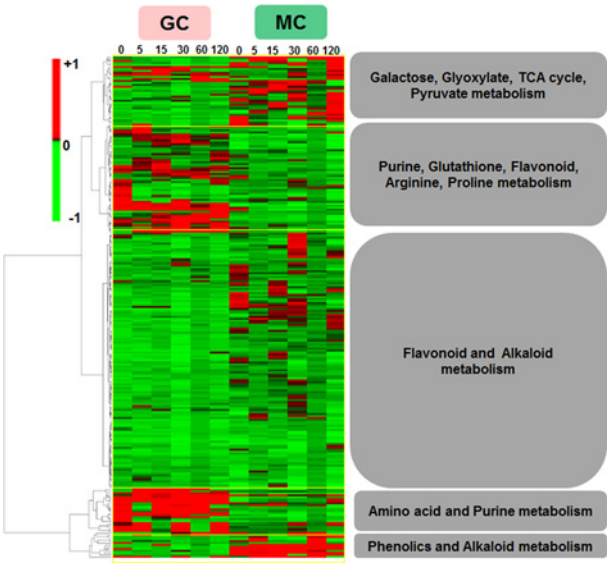

Fig 2. Hierarchical cluster analysis (HCA) of mean values of metabolite contents from four biological replicates showing 268 metabolites common to the two cell-types depicting the data structure dependent on the cell-types and time course (0–120 mpi) of HCO_3^- treatment. Red and green indicate high and low concentrations of metabolites, respectively. Values were subjected to average linkage clustering (Euclidean distance). Outlined blocks in yellow show grouped metabolites in the two cell-types.

doi:10.1371/journal.pone.0144206.g002

in GCs compared to the MCs. The largest and third cluster grouped metabolites of mostly secondary metabolism origin and belonged to flavonoid and alkaloid biosynthesis, which showed increases in MCs and sharp decreases in GCs. The last two small clusters contained amino acid and purine metabolites with increases in GCs, and phenylpropanoid and alkaloid metabolites with increases in MCs.

In the short time-series expression miner (STEM) analysis, a model significantly explained the constantly increasing accumulation pattern of 27 metabolites in MCs (enriched in galactose, flavonoid, and pyruvate metabolism) (Fig 3A), whereas in GCs another model significantly explained the constantly decreasing pattern of 39 metabolites (enriched in pyrimidine, alanine, beta-alanine, aspartate, glutamate, pantothenate, and nitrogen metabolism) (Fig 3B) during the time-course. While a few of the models demonstrated clear and linear patterns of changes, and a majority of the metabolites showed mostly 'biphasic' patterns with two peaks and two troughs.

Global and pathway-wise metabolic responses to HCO_3^- treatment in GCs and MCs

PCA using an unsupervised multivariate linear model revealed grouped and differential responses of the cell-types to HCO_3^- with an interpretable visualization. The resulting plots for MCs explained 54% variations by two PCs (PC1- 39% and PC2-15%) attributed to the variations from the HCO_3^- treatment and time course components (Fig 4A). On the other hand, the resulting plots for GCs explained 72% variations by two PCs (PC1-54% and PC2-18%) attributed to the variations from the HCO_3^- treatment and time course components (Fig 4B). The effect of time (Fig 4C) and treatment x time (Fig 4D) were also discernible using the global PCA. A supervised approach of classification, OPLS-DA analysis was conducted to indicate grouped responses of the cell-types to treatment and time-course for both MCs and GCs. The

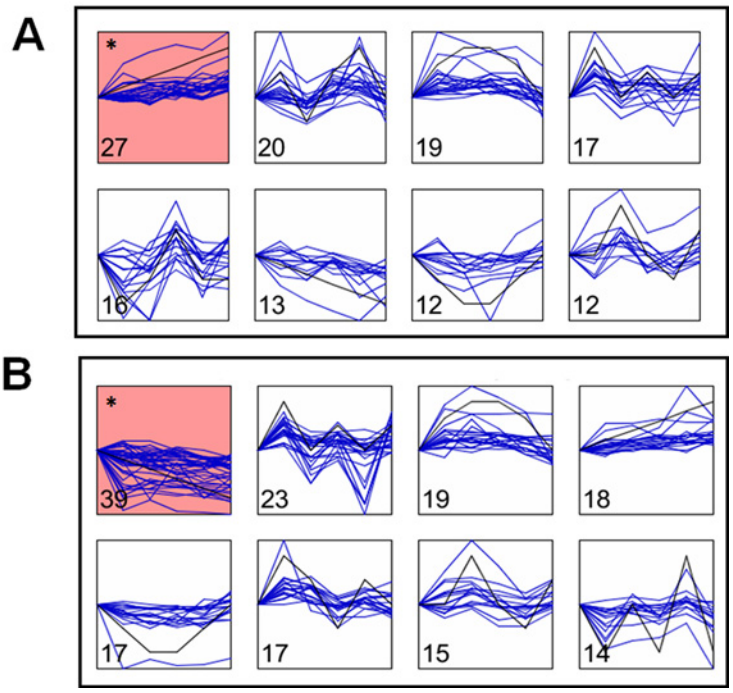

Fig 3. STEM analysis showing metabolite accumulation patterns across the time-course of HCO_3^- treatment of (A) MC and (B) GC. Numbers at the bottom-left indicate the metabolites with similar trends, and the star indicates significance ($P < 0.05$).

doi:10.1371/journal.pone.0144206.g003

grouped responses of cell-type x treatment x time are shown for the two cell-types (Fig 4E and 4F).

In our metabolomic analyses, 26 and 27 metabolites in MCs and GCs were uniquely identified, respectively, to be enriched with sugar alcohols, phytohormones, organic acids, and aromatic amino acid metabolism in MCs and sugar alcohols, flavonoids, organic acids, sugars, and fatty acid in GCs (S4 Fig). Out of the unique metabolites, glycine, proline, and ABA showed significant increases at 5 mpi in MCs, while ethylene glycol, myricetin, niacin, suberylglycine, succinic semialdehyde, and uric acid showed significant decreases at 60 mpi in GCs (S4 Fig). In addition, the number of increased metabolites outnumbered the decreased in the two cell-types (S5 Fig), which corroborated the recent transcriptomic findings [43]. Furthermore, there more number of significantly changed metabolites in GCs than in MCs (S2 Fig). Hence, we looked at the major metabolic pathways in both cell-types to gauge the impact of treatment. Changes in amino acids demonstrate a very clear increased accumulation in MCs as compared to decreases in GCs (Fig 5). This preference of MCs for C-incorporation into N metabolism is opposite to GC response in decreased N-accumulation. Significant increases and decreases in cysteine levels were observed in MCs and GCs, respectively. Pyroglutamate and o-phosphoserine showed opposite trends in the cell-types, i.e., significant decreases in MCs and increases in GCs. In terms of primary metabolism, which centers on the central C-metabolism, the TCA cycle remained unchanged attributable to high fluxes in the cycle (Fig 5). However, in GCs, the continual and significant increase of malate at all time-points of HCO_3^- treatment indicates induction of glyoxylate cycle thus leading to gluconeogenesis. These elevated glyoxysomal responses are further supported by continually elevated succinic acid in the GCs (S5 Fig), which is released during acetyl CoA utilization and used in carbohydrate biosynthesis. However, the photosynthesis-related metabolites showed increasing trends in MCs and opposite trends in

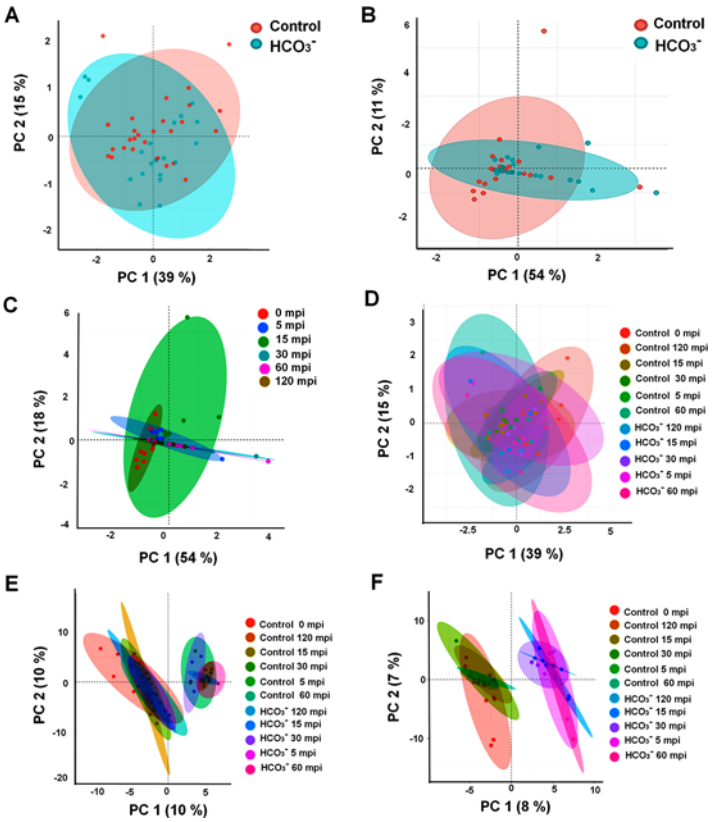

Fig 4. Principal component analysis (PCA) and orthogonal partial least square discriminant (OPLS-DA) analysis of metabolite changes in GCs and MCs after HCO_3^- treatment. PCA was performed using four replicate data of relative metabolite abundances in the cell-types at 0, 5, 15, 30, 60, 120 mpi, and the generated PC1 and PC2 were plotted. PCA of two cell-types showing a clear separation of the two groups based on the 268 metabolites for the effect of treatments in (**A**) GCs, and (**B**) MCs. The effects of only **(C)** time and both (**D**) 'treatment x time' were displayed. In OPLS-DA, the metabolite changes as a result of interactions among 'cell-type x treatment x time were displayed in **(E)** GCs and (**F**) MCs.

doi:10.1371/journal.pone.0144206.g004

GCs. In contrast, the GCs showed higher accumulation of pentose phosphate pathway metabolites than MCs. Following the same patterns, starch and sucrose metabolites, and amino and nucleotide sugar metabolites in GCs showed significantly higher accumulation than in MCs. In GCs, fructose, glucose, and mannose showed increases during the early time-points, while kestose, maltose, and isomaltose showed sustained increases throughout the time course (Fig 5). In contrast, changes of the above metabolites in MCs were not significant. Another important and large pool of cellular N-metabolites contained purines and pyrimidines. In GCs, increases in purine metabolism are clearly visible during the entire time-course, whereas pyrimidine metabolism showed mixed responses across the time-points. On the other hand, in MCs purine metabolites were constantly decreased throughout the time-course, except for 15 mpi (Fig 5; S7 Table). In addition, the pentose phosphate pathway metabolites that are interconnected to purine and pyrimidine metabolism, i.e., glucose-6-phosphate and ribose-5-phosphate levels showed increased accumulation in GCs throughout the time-course, indicating the need for cellular energy (NADPH and ATP) for stomatal movement. On the other hand, this response was opposite in MCs where these two metabolites were decreased. Over all, the changes in purine and pyrimidine metabolites showed clear increases in GCs (Fig 6). Secondary metabolites play important roles in plant defense responses and are derived from primary C-and N-

Fig 5. Responses of major metabolite groups in MCs and GCs upon HCO_3^- treatment in the time-course study. Green and red squares indicate decreased (<0.8) and increased (>1.2) fold changes, respectively. The asterisks indicate significant changes (P <0.05).

doi:10.1371/journal.pone.0144206.g005

metabolism. In both cell-types, alkaloid biosynthesis related metabolites showed increases throughout the time-course, while in MCs phenylpropanoids showed increased levels (Fig 6). Epicatechin and 4-methylgenistein showed significant increase and decrease, respectively, in GCs. In addition, catechin and coumaric acid showed significant increases in GCs throughout the time-course. In MCs except 2,3-dihydroxybenzoic acid that showed significant increases throughout the time-course, no other metabolites showed significant changes (Fig 5). Moreover, GCs at 5 mpi, 15 mpi, and 30 mpi showed decreases in aromatic amino acids (tyrosine, phenylalanine, and tyrosine). These treatment-correlated metabolites indicate that the HCO_3^--induced metabolic reprogramming involved the phenylpropanoid pathway and its branches such as flavonoid biosynthetic pathway. In addition, a clear remodeling of the phytohormonal status in both GCs and MCs was evident in HCO_3^- treated cell-type metabolome, indicating increases in the majority of phytohormones in MCs and decreases in auxins and cytokinins in GCs (Fig 5). Interestingly, JA first increased in GCs, and then decreased at the later time-points

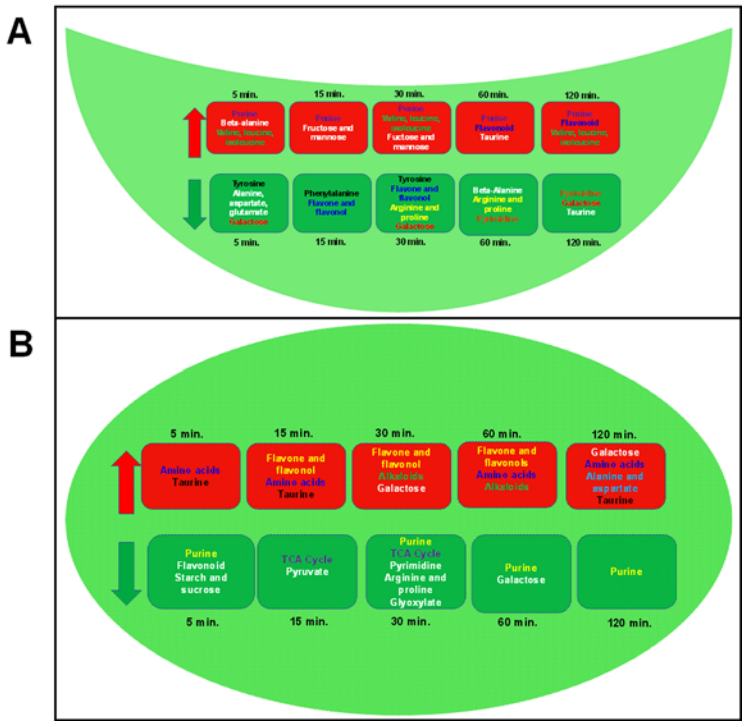

Fig 6. Summary of the increased and decreased metabolic pathways in (A) GCs and (B) MCs after HCO_3^- treatment.

doi:10.1371/journal.pone.0144206.g006

thus coinciding with the stomatal closure (Fig 1). In contrast, the JA levels remained unchanged in MCs. Similarly, SA, kinetins (zeatin, zeatin riboside, and kinetin) and auxins (IAA and IBA) decreased in GCs, but increased in MCs. Only gibberellin content increased in GCs, and remained unchanged in MCs (Fig 6). Furthermore, HCO_3^- treatment caused in GCs significantly increased GSH and decreased GSSG, dehydroascorbic acid, cysteine, cysteine-S-sulfate, and N-formylmethioine. In contrast, MCs contained more oxidized metabolites largely due to their increased photosynthesis and light-induced oxidation in the presence of high CO_2 (Fig 5).

Discussion

Metabolomic insights into differential HCO_3^- perception and conversion by GCs and MCs

Carbonic anhydrase converts CO_2 into HCO_3^- for incorporation into cellular metabolism [44] and acts as an upstream regulator of CO_2 controlled stomatal movement [45–47]. Estimates indicate that at least 250 μM HCO_3^- is present in the cytosol of a leaf cell in ambient air [48], maintained by cytosolic CA activity. Thus, the HCO_3^- concentration used for the treatment is in excess. Photosynthesis is generally enhanced by elevated CO_2, and leading to high accumulation of photosynthates [17, 49]. Furthermore, GC photosynthesis is critical for stomatal turgor production, but it does not mediate CO_2 or ABA-induced stomatal closure [50]. With single-cell type metabolomics, we showed differential accumulation levels of metabolites in MCs and GCs, highlighting the power of single-cell type metabolomics in improving the resolution of tissue level metabolic changes [6]. Clearly, MCs contribute to the bulk of leaf metabolism and biosynthesis, whereas GCs present their unique metabolic repertoire for stomatal responses to environmental cues that range from pathogen to CO_2. In GCs, the elevated HCO_3^-, more so

than elevated CO_2, alters the intracellular free calcium ion [Ca^{2+}] sensitivity of SLAC1, leading to reduced stomatal opening [51]. In most non-photosynthetic tissues and the photosynthetic tissues of C3 plants, phosphoenolpyruvate carboxylase (PEPCase) catalyzes the conversion of phosphoenolpyruvate (PEP) and HCO_3^- to oxaloacetate, i.e., to replenish TCA cycle intermediates in addition to malate production in guard cells [52]. Maintaining the cellular C/N balance in plants is complex and multiple mechanisms are involved [53, 54] to accommodate metabolome-wide changes.

In GCs, more metabolites showed HCO_3^- responsiveness than in MCs as the capacity for metabolite flux through the catabolic pathways is high in GCs compared to MCs [55]. In addition, stomata and MCs play different roles in conducting CO_2 to the sites of carboxylation in chloroplasts, as GCs are known to present higher PEPCase activities than MCs [56]. Thus, the large number of metabolites showing HCO_3^- responsiveness in GCs may be due to high metabolic rates in different pathways. In fact, MCs are known to be involved primarily in photosynthate production, while GCs are gate keepers for air and water exchange, in addition to forming the first line of defense against pathogens. Thus, stomatal closure in response to increased HCO_3^- helps to protect MCs from possible overloading. Increased accumulation of amino acids, phenylpropanoids, and redox metabolites in MCs contrasts with decreased accumulation of amino acids and increased accumulation of sugars, pentose phosphate pathway, and purine metabolites in GCs, reflecting the inherent functional dichotomy (Figs 5 and 6). Glutamate occupies a central position in amino acid metabolism and plays a central signaling and metabolic role at the interface of the C and N assimilatory pathways [57]. The decrease of glutamate in GCs (Fig 3B) reiterates the subdued amino acid metabolism. On the other hand, the boost in overall nitrogen metabolites in MCs reflects the primary functional role of MCs in incorporation of excess CO_2 into N-metabolism. In contrast, GCs prominently direct carbon into sugars and pentose phosphate metabolites for energy. Our results further reflect the mutual dependency of GCs on MCs for cellular maintenance and regulatory functions.

HCO_3^- triggered changes in purine and specialized metabolism in MCs and GCs

Nitrogenous bases in the form of purines and pyrimidines form an essential pool of nitrogen in plant cells [58, 59] as metabolic intermediates, and signaling molecules in guard cell functions [9]. For instance, cyclic adenosine diphosphoribose (cADPR), a purine derived from nicotinamide adenine dinucleotide (NAD), plays important roles in guard cell ABA signaling. Injection of cADPR into guard cells resulted in [Ca^{2+}] increases and turgor reduction [60]. Another purine, cyclic guanosine monophosphate (cGMP), has been implicated in ABA-induced stomatal closure by acting downstream of H_2O_2 and NO in the ABA signaling pathway [61]. The nitrated form of cGMP (8-nitro-cGMP) is a positive regulator in promotion of stomatal closure [62]. Moreover, increased accumulation of adenosine, inosine, and guanosine-derived metabolites in GCs was opposite to their decreased pattern in MCs, indicating their differential responses to elevated CO_2. Pyrimidine metabolism operates mostly in plastids to provide intermediates for lipid and carbohydrate synthesis [63]. Decreased pyrimidine levels in GCs at later time-points indicate their possible utilization for the biosynthesis of lipids and sugars.

Phenylpropanoids are known in the context of plant stress and defense responses as they demonstrate a significant time-dependent accumulation [64]. MC-specific increases of phenylpropanoids as compared to GCs indicate that MCs may be the biosynthetic hubs for plant foliar defense systems as a result of phenylpropanoid accumulation [65, 66]. Transcripts involved in stress-responsive functions are known to be highly induced upon elevated CO_2 treatment [43]. Flavonoids biosynthesis is downstream of phenylpropanoid metabolism.

Although more prominent in GCs, comparable increases of flavonoids in both cell-types were noted (Figs 2 and 5). The presence of dihydroxy B-ring substituted flavonoids in the nucleus of MCs was reported [67], but their role other than protection from oxidative damage is unknown. Although the involvement of flavonoids in stomatal movement is known [9, 68], changes in flavonoid metabolism in response to elevated CO_2 at the cellular levels have not been reported [69]. Evidently, the role of flavonoids such as kaempferol and quercetin in GCs is to protect from ROS induced stomatal closure [68]. Furthermore, in bread wheat [3] and strawberry [69] the accumulation of flavonoids increased upon elevated CO_2 as compared to plants under ambient CO_2. Similarly, elevated CO_2 resulted in increased alkaloids by altering the C/N balance toward a positive effect on biosynthesis of these metabolites [70]. Under elevated CO_2, high levels of morphine, codeine, papaverine, and noscapine were produced in wild poppy (*Papaver setigerum*) [71], and scopolamine was accumulated in jimson weed (*Datura stramonium* L.) [72]. In this study, we observed increased alkaloid biosynthetic pathway intermediates in both GCs and MCs. The increased specialized metabolites in both cell-types upon CO_2 elevation may indicate increased primary metabolites/photosynthates, and signaling roles, e.g., in GCs.

Redox state and phytohormone changes in HCO_3^- treated MCs and GCs

NO is known to be a signaling intermediate in 2 mM HCO_3^- induced stomatal closure in *Pisum sativum* [27], while ascorbate is known to be dramatically decreased by high CO_2 in plants [19]. In this study, we showed that 1 mM HCO_3^- induced stomatal closure (Fig 1). Although less severe in C3 plants, increased oxidative stress was found in plants grown under elevated CO_2 [73, 74]. In addition, up-regulation of genes encoding enzymes involved in oxidative signaling and ROS scavenging such as glutathione-S-transferase, peroxidases, catalases, cysteine and thioredoxin-pathway related genes was reported [43]. Elevated CO_2 can enhance maintenance of the redox potential due to an elevated rate of CO_2 assimilation and low photorespiration [75]. Through H_2O_2 production and pyridine nucleotide interactions, photorespiration makes a key contribution to cellular redox homeostasis [76, 77]. Increased redox metabolites (e.g., homocysteine, methionine, methionine sulfone, N-formylmethionine, dehydroascorbate, glucoronate, gamma-glu-cys, and cystathionine) in MCs and their decreased and opposite accumulation patterns in GCs corroborate the role of redox state in GC signaling and stomatal movement [78]. Furthermore, the role of sulfur metabolites in GC signaling and movement has generated considerable interest. For instance, the role of sulfur dioxide (SO_2) in NO and ROS-mediated apoptosis induction in the GCs of different species has been established [79–81]. Although changes of major phytohormones in response to stomatal ABA signaling were studied using metabolomic approaches [8], elevated CO_2 is known to enhance the activities of ABA-independent enzyme, carbonic anhydrase, leading to further decrease in stomatal aperture [82]. Elevated CO_2 is known to stimulate the SA pathway but repress the JA pathway in plants [83], as elevated CO_2 may cause plants to re-allocate resources for SA synthesis and SA/JA crosstalk [84, 85]. Plant hormone signaling pathways related to defense are interconnected through complex regulatory networks [86]. In recently available transcriptomic data of moss gametophytes exposed to elevated CO_2, up-regulation of ABA, JA, brassinosteroid, and ethylene metabolism-related genes was observed [43]. Similar instances were reported in *A. thaliana* challenged with elevated CO_2 [14]. Not surprisingly, as foliar photosynthetic cells (i.e., MCs) form the bulk tissue in plants, the averaged leaf metabolic data share similarities to MC responses [14, 43]. Analysis of physiological and morphological stomatal responses of several species suggests that patterns of stomatal responses to CO_2 do not follow a phylogenetic pattern associated with plant evolution [87]. This interesting phenomenon deserves further investigation using the specific cell-types and metabolomics approaches reported in this study.

Conclusions

As time-resolved single-cell type metabolomic studies are rare, the HCO_3^- induced metabolomic changes reported here in the two important cell-types help us understand high CO_2-mediated short-term metabolomic responses in GCs and MCs. The responsiveness of the cells to HCO_3^- is characterized by specific metabolites grouped by functional and temporal behavior. In MCs the increased metabolites outnumber the increased metabolites in GCs, where a comparable number of metabolites showed decreasing patterns. Moreover, the metabolomic responses of MCs showed contrasting patterns to GCs in amino acid, purine, phytohormone, and flavonoid metabolism in response to elevated HCO_3^-, which reflects the differential metabolic predisposition and responses to the stimulus. Hence, the results in this study have shown utility of metabolomics tools towards improved understanding of the plant CO_2 sensing and response mechanisms. The data may be useful to predict plant responses and productivity in an ever changing climate. In addition, efforts are underway to enhance C3 carbon concentrating mechanism in chloroplasts by adding more bicarbonate transporters to increase bicarbonate flux into plastids for enhanced carbon fixation [88–90]. We are fully aware that GCs are not autonomously regulated, and there is a strong link between MC metabolism and stomata function [91, 92]. Focused studies on the interactions between MCs and GCs are underway in our laboratories.

Supporting Information

Additional Supporting Information may be found in the online version of this article at the publisher's web-site:

S1 Fig. Total metabolites quantified mapped onto KEGG metabolic pathways. Using targeted HPLC-MRM-MS and GC-MS platforms, a total of 268 metabolites (shown as red dots) were quantified and mapped onto KEGG pathways.
(TIF)

S2 Fig. Volcano plots displaying differential changes of metabolite levels in MCs at different time-points of HCO_3^- treatment compared to respective controls. (A) 5 mpi, (B) 15 mpi, (C) 30 mpi, (D) 60 mpi, and (E) 120 mpi HCO_3^- treatment. Metabolites are ranked according to their statistical–log10 (P-value) (y-axis) and log 2 (fold change) (x-axis). Cut-offs were P-values < 0.05 and fold changes > 1.2 or < 0.8. Off-centered metabolites are those that varied the most between the two treatment conditions.
(TIF)

S3 Fig. Volcano plots displaying differential changes of metabolite levels in GCs at different time-points of HCO_3^- treatment compared to respective controls. (A) 5 mpi, (B) 15 mpi, (C) 30 mpi, (D) 60 mpi, and (E) 120 mpi HCO_3^-. Metabolites are ranked according to their statistical–log10 (P-value) (y-axis) and log 2 (fold change) (x-axis). Cut-offs were P-values < 0.05 and fold changes > 1.2 or < 0.8. Off-centered metabolites are those that varied the most between the two treatment conditions.
(TIF)

S4 Fig. Uniquely identified metabolites in the two cell-types. (A) MCs and (B) GCs. Abbreviations used: ME: methyl ester, 2H4MAP: 2-hydroxy4-methoxyacetophenone.
(TIF)

S5 Fig. Total increased, decreased, and significantly changed metabolites during the time-course profiling study. (A) MCs and (B) GCs. Significantly changed metabolites include both

increased and decreased metabolites at a given time-point.
(TIF)

S1 Table. Metabolites used in the time-course profiling study for the targeted analysis by HPLC-MRM-MS/MS. KEGG: Kyoto Encyclopedia of Genes and Genomes, HMDB: Human Metabolome Database, InChI Key: IUPAC International Chemical Identifier, CAS: Chemical Abstracts Service (CAS) number, ESI: Electron Spray Ionization, Q1:Precursor Ion, Q2: Daughter Ion (Transition), DP: Declustering Potential, CE: Collision Energy, CXP: Cell Exit Potential (10 and -10 for positive and negative modes for the 4000 QTRAP (ABSciex) used.
(XLSX)

S2 Table. Raw metabolomic data sets. Peak areas (as relative abundances) of metabolites quantified using combined GC-MS and HPLC-MRM-MS/MS analyses at 0, 5, 15, 30, 60, and 120 mpi bicarbonate treatment (T) and control (C) for GCs and MCs (n = 4).
(XLSX)

S3 Table. Processed metabolomic data sets for MCs. Fold changes (1.2 and 0.8 as cut-offs) and significantly changed MC metabolites ($P < 0.05$) at 5, 15, 30, 60 and 120 mpi bicarbonate treatment with respect to controls as inferred from ANOVA.
(XLSX)

S4 Table. Processed metabolomic data sets for GCs. Fold changes (1.2 and 0.8 as cut-offs) and significantly changed GC metabolites ($P < 0.05$) at 5, 15, 30, 60, and 120 mpi bicarbonate treatment (T) with respect to controls (C) as inferred from ANOVA.
(XLSX)

S5 Table. Significantly changed metabolites in the cell-types as inferred by within subject ANOVA. Significantly changed metabolites ($P < 0.05$) for (A) GC and (B) MC at 5, 15, 30, 60 and 120 mpi bicarbonate treatment with respect to controls as inferred from within subject ANOVA models.
(XLSX)

S6 Table. Significantly changed metabolites in two cell-types. Significantly changed metabolites (P-value< 0.05) for (A) GC and (B) MC at 5, 15, 30, 60 and 120 mpi bicarbonate treatments with respect to controls.
(XLSX)

S7 Table. Pathway enrichment of changed metabolites in the two cell-types. Pathway enrichment for (A) GC and (B) MC metabolites showing increases or decreases after 5, 15, 30, 60, and 120 mpi bicarbonate treatment.
(XLSX)

Acknowledgments

Dr. Fei Wang in the Tong lab is thanked for technical assistance with GC-MS analysis. This work was supported by the U.S. National Science Foundation grant MCB-1158000 to SC.

Author Contributions

Conceived and designed the experiments: SC BM. Performed the experiments: BM EA ZT. Analyzed the data: BM. Contributed reagents/materials/analysis tools: SC EA ZT. Wrote the paper: BM SC.

References

1. IPCC. Climate change 2013: the physical science basis. Working Group I contribution to the Intergovernmental Panel on Climate Change. 2013. (http://www.ipcc.ch/report/ar5/wg1/#.Ulay4VAqjwF) *Accessed on 7th July, 2015*.
2. Long SP, Ainsworth EA, Leakey ADB, Nösberger J, Ort DR. Food for thought: lower-than-expected crop yield stimulation with rising CO_2 concentrations. Science 2006; 312: 1918–1921. PMID: 16809532
3. Levine LH, Kasahara H, Kopka J, Erban A, Fehrl I, Kaplan F. et al. Physiologic and metabolic responses of wheat seedlings to elevated and super-elevated carbon dioxide. Adv. Space Res. 2008; 42: 1917–1928.
4. Ainsworth EA, Rogers A. The response of photosynthesis and stomatal conductance to rising [CO_2]: mechanisms and environmental interactions. Plant Cell Environ. 2007; 30: 258–270. PMID: 17263773
5. Ainsworth EA, Leakey AD, Ort DR, Long SP. FACE-ing the facts: inconsistencies and interdependence among field, chamber and modeling studies of elevated [CO_2] impacts on crop yield and food supply. New Phytol. 2008; 179: 5–9. doi: 10.1111/j.1469-8137.2008.02500.x PMID: 18482226
6. Misra BB, Assmann SM, Chen S. Plant single-cell and single-cell-type metabolomics. Trends Plant Sci. 2014; 19: 637–646. doi: 10.1016/j.tplants.2014.05.005 PMID: 24946988
7. Medeiros DB, Daloso DM, Fernie AR, Nikoloski Z, Araújo WL. Utilizing systems biology to unravel stomatal function and the hierarchies underpinning its control. Plant Cell Environ. 2015 doi: 10.1111/pce.12517
8. Jin X, Wang RS, Zhu M, Jeon BW, Albert R, Chen S, Assmann SM Abscisic acid–responsive guard cell metabolomes of *Arabidopsis* wild-type and *gpa1* G-protein mutants. Plant Cell 2013; 25:4789–4811. doi: 10.1105/tpc.113.119800 PMID: 24368793
9. Misra BB, Acharya BR, Granot D, Assmann SM, Chen S. The guard cell metabolome: Functions in stomatal movement and global food security. Front Plant Sci. 2015; 6: 334. doi: 10.3389/fpls.2015.00334 PMID: 26042131
10. Prior SA, Pritchard SG, Runion GB. Leaves and the effects of elevated carbon dioxide levels. Dekker Encyclopedia of Plant and Crop Science 2004; 648–650.
11. Ainsworth EA, Long SP. What have we learned from 15 years of free-air CO_2 enrichment (FACE)? A meta-analytic review of the responses of photosynthesis, canopy properties and plant production to rising CO_2. New Phytol. 2005; 165: 351–372. PMID: 15720649
12. Long SP, Ainsworth EA, Rogers A, Ort DR. Rising atmospheric carbon dioxide: plants FACE the future. Annu. Rev. Plant Biol. 2004; 55: 591–628. PMID: 15377233
13. Li P, Ainsworth EA, Leakey AD, Ulanov A, Lozovaya V, Ort DR, et al. *Arabidopsis* transcript and metabolite profiles: ecotype-specific responses to open-air elevated [CO_2]. Plant Cell Environ. 2008; 31: 1673–1687. doi: 10.1111/j.1365-3040.2008.01874.x PMID: 18721265
14. Kaplan F, Zhao W, Richards JT, Wheeler RM, Guy CL, Levine LH. Transcriptional and metabolic insights into the differential physiological responses of *Arabidopsis* to optimal and supraoptimal atmospheric CO_2. PLoS One 2012; 7: e43583. doi: 10.1371/journal.pone.0043583 PMID: 22916280
15. Fukayama H, Sugino M, Fukuda T, Masumoto C, Taniguchi Y, Okada M, et al. (2011) Gene expression profiling of rice grown in free air CO_2 enrichment (FACE) and elevated soil temperature. Field Crops Res. 2011; 121: 195–199.
16. Tallis MJ, Lin Y, Rogers A, Zhang J, Street NR, Miglietta F, et al. (2010) The transcriptome of *Populus* in elevated CO_2 reveals increased anthocyanin biosynthesis during delayed autumnal senescence. New Phytol. 2010; 186: 415–428. doi: 10.1111/j.1469-8137.2010.03184.x PMID: 20202130
17. Geissler N, Hussin S, Koyro HW. Elevated atmospheric CO_2 concentration enhances salinity tolerance in *Aster tripolium* L. Planta 2009; 231: 583–594. doi: 10.1007/s00425-009-1064-6 PMID: 20072826
18. Papadimitropoulos MEP, Klapa MI. Investigating the effect of elevated CO_2 in the growth environment of salt-stressed plants using integrated omic analyses. In Combined Stresses in Plants (pp. 49–69). 2015; Springer International Publishing.
19. Miyagi A, Takahara K, Kasajima I, Takahashi H, Kawai-Yamada M, Uchimiya H. Fate of ^{13}C in metabolic pathways and effects of high CO_2 on the alteration of metabolites in *Rumex obtusifolius* L. Metabolomics 2011; 7: 524–535.
20. Beardall J, Johnston A, Raven J. Environmental regulation of CO_2-concentrating mechanisms in microalgae. Can. J. Bot. 1998; 76: 1010–1017.
21. Renberg L, Johansson AI, Shutova T, Stenlund H, Aksmann A, Raven JA, et al. A metabolomic approach to study major metabolite changes during acclimation to limiting CO_2 in *Chlamydomonas reinhardtii*. Plant Physiol. 2010; 154: 187–196. doi: 10.1104/pp.110.157651 PMID: 20634393

22. Fang W, Si Y, Douglass S, Casero D, Merchant SS, Pellegrini M, et al. Transcriptome-wide changes in *Chlamydomonas reinhardtii* gene expression regulated by carbon dioxide and the CO_2-concentrating mechanism regulator CIA5/CCM1. Plant Cell 2012; 24: 1876–1893. doi: 10.1105/tpc.112.097949 PMID: 22634760

23. Baba M, Suzuki I, Shiraiwa Y. Proteomic analysis of high-CO_2-inducible extracellular proteins in the unicellular green alga, *Chlamydomonas reinhardtii*. Plant Cell Physiol. 2011; 52: 1302–1314. doi: 10.1093/pcp/pcr078 PMID: 21680606

24. Daloso DM, Antunes WC, Pinheiro DP, Waquim JP, Araújo WL, Loureiro ME, et al. Tobacco guard cells fix CO_2 by both RubisCO and PEPCase whilst sucrose acts as a substrate during light induced stomatal opening. Plant Cell Environ. 2015. doi: 10.1111/pce.12555

25. Assmann SM. The cellular basis of guard cell sensing of rising CO_2. Plant Cell Environ 1999; 22: 629–637.

26. Ramanam R, Nadimuthu V, Saravana Devi S, Krishnamurthi K, Tapan C. Influence of CO_2 concentration on carbon concentrating mechanisms in cyanobacteria and green algae: a proteomic approach. Algae 2012; 27: 295–301.

27. Kolla VA, Raghavendra AS. Nitric oxide is a signaling intermediate during bicarbonate-induced stomatal closure in *Pisum sativum*. Physiol. Plant. 2007; 130: 91–98.

28. Mrinalini T, Latha YK, Raghavendra AS, Das VSR. Stimulation and inhibition by bicarbonate of stomatal opening in epidermal strips of *Commelina benghalensis*. New Phytol. 1982; 91: 413–418.

29. Kolla VA, Vavasseur A, Raghavendra AS. Hydrogen peroxide production is an early event during bicarbonate induced stomatal closure in abaxial epidermis of *Arabidopsis*. Planta 2007; 225: 1421–1429. PMID: 17160388

30. Chen S, Halkier BA. Characterization of glucosinolate uptake by leaf protoplasts of *Brassica napus*. J. Biol. Chem. 2000; 275: 22955–22960. PMID: 10816580

31. Grapov D. DeviumWeb: version 0.3.2. ZENODO. 2014. doi: 10.5281/zenodo.12879, https://github.com/dgrapov/DeviumWeb

32. Fiehn O, Wohlgemuth G, Scholz M, Kind T, Lee DY, Lu Y. et al. Quality control for plant metabolomics: reporting MSI-compliant studies. Plant J. 2008; 53: 691–704. doi: 10.1111/j.1365-313X.2007.03387.x PMID: 18269577

33. Chen W, Gong L, Guo Z, Wang W, Zhang H, Liu X, et al. A novel integrated method for large-scale detection, identification, and quantification of widely targeted metabolites: application in the study of rice metabolomics. Mol. Plant 2013; 6: 1769–1780. doi: 10.1093/mp/sst080 PMID: 23702596

34. Lisec J, Schauer N, Kopka J, Willmitzer L, Fernie AR. Gas chromatography mass spectrometry-based metabolite profiling in plants. Nat. Protoc. 2006; 1: 387–396. PMID: 17406261

35. Stein SE. An integrated method for spectrum extraction and compound identification from gas chromatography/mass spectrometry data. J. Am. Soc. Mass Spectrom. 1999; 10: 770–781.

36. Kopka J, Schauer N, Krueger S, Birkemeyer C, Usadel B, Bergmüller E, et al. GMD@ CSB. DB: the Golm metabolome database. Bioinformatics 2005; 21: 1635–1638. PMID: 15613389

37. Sokal RR, Rohlf FJ. Biometry: The principles and practice of statistics in biological research. New York: W.H. Freeman and Company 1995;337.

38. Benjamini Y, Hochberg Y. Controlling the false discovery rate—a practical and powerful approach to multiple testing. J R Stat. Soc. Series B Stat. Methodol. 1995; 57: 289–300.

39. Caraux G, Pinloche S. PermutMatrix: a graphical environment to arrange gene expression profiles in optimal linear order. Bioinformatics 2005; 21: 1280–1281. PMID: 15546938

40. Kuehn H, Liberzon A, Reich M, Mesirov JP. Using GenePattern for gene expression analysis. Curr. Protoc. Bioinformatics 2008;7–12.

41. Xia JG, Psychogios N, Young N, Wishart DS. MetaboAnalyst: a web server for metabolomic data analysis and interpretation. Nucleic Acids Res. 2009; 37: W652–W660. doi: 10.1093/nar/gkp356 PMID: 19429898

42. Ernst J, Bar-Joseph Z. STEM: a tool for the analysis of short time series gene expression data. BMC Bioinformatics 2006; 7: 191. PMID: 16597342

43. Shinde S, Behpouri A, McElwain JC, Ng CKY. Genome-wide transcriptomic analysis of the effects of sub-ambient atmospheric oxygen and elevated atmospheric carbon dioxide levels on gametophytes of the moss, *Physcomitrella patens*. J. Exp. Bot. 2015;erv197. doi: 10.1093/jxb/erv197

44. Tian W, Hou C, Ren Z, Pan Y, Jia J, Zhang H, et al. A molecular pathway for CO_2 response in *Arabidopsis* guard cells. Nat. Commun. 2015; 6: 6057. doi: 10.1038/ncomms7057 PMID: 25599916

45. Hu H, Boisson-Dernier A, Israelsson-Nordström M, Böhmer M, Xue S, Ries A, et al. Carbonic anhydrases are upstream regulators of CO2-controlled stomatal movements in guard cells. Nature Cell Biol. 2010; 12: 87–93. doi: 10.1038/ncb2009 PMID: 20010812

46. Hu H, Rappel WJ, Occhipinti R, Ries A, Böhmer M, You L, et al. Distinct cellular locations of carbonic anhydrases mediate CO_2 control of stomatal movements. Plant Physiol. 2015; p00646. doi: http://dx.doi.org/10.1104/pp.15.00646

47. Matrosova A, Bogireddi H, Mateo-Peñas A, Hashimoto-Sugimoto M, Iba K, Schroeder JI, et al. The HT1 protein kinase is essential for red light-induced stomatal opening and genetically interacts with OST1 in red light and CO_2-induced stomatal movement responses. New Phytol. 2015. doi: 10.1111/nph.13566

48. Evans JR, Von Caemmerer S. Carbon dioxide diffusion inside leaves. Plant Physiol. 1996; 110: 339. PMID: 12226185

49. Li X, Zhang G, Sun B, Zhang S, Zhang Y, Liao Y, et al. Stimulated leaf dark respiration in tomato in an elevated carbon dioxide atmosphere. Sci. Rep. 2013; 3: 3433. doi: 10.1038/srep03433 PMID: 24305603

50. Azoulay-Shemer T, Palomares A, Bagheri A, Israelsson-Nordstrom M, Engineer CB, Bargmann BO, et al. Guard cell photosynthesis is critical for stomatal turgor production, yet does not directly mediate CO_2-and ABA-induced stomatal closing. Plant J. 2015; 83: 567–581. doi: 10.1111/tpj.12916 PMID: 26096271

51. Xue SW, Hu HH, Ries A, Merilo E, Kollist H, Schroeder JI. Central functions of bicarbonate in S-type anion channel activation and OST1 protein kinase in CO_2 signal transduction in guard cell. EMBO J. 2011; 30: 1645–1658. doi: 10.1038/emboj.2011.68 PMID: 21423149

52. Chollet R, Vidal J, O'Leary MH. Phosphoenolpyruvate carboxylase: a ubiquitous, highly regulated enzyme in plants. Annu. Rev. Plant Biol. 1996; 47: 273–298.

53. Scheible WR, Gonzalez-Fontes A, Lauerer M, Muller-Rober B, Caboche M, Stitt M. Nitrate acts as a signal to induce organic acid metabolism and repress starch metabolism in tobacco. Plant Cell 1997; 9: 783–798. PMID: 12237366

54. Lammertyn J, Franck C, Verlinden BE, Nicolaï BM. Comparative study of the O_2, CO_2 and temperature effect on respiration between 'Conference' pear cell protoplasts in suspension and intact pears. J. Exp. Bot. 2011; 52: 1769–1777.

55. Hampp R, Outlaw WH, Tarczynski MC. Profile of basic carbon pathways in guard cells and other leaf cells of *Vicia faba* L. Plant Physiol. 1982; 70: 1582–1585. PMID: 16662723

56. Düring H. Stomatal and mesophyll conductances control CO_2 transfer to chloroplasts in leaves of grapevine (*Vitis vinifera* L.). VITIS-J. Grapevine Res. 2015; 42: 65.

57. Forde BG, Lea PJ. Glutamate in plants: metabolism, regulation, and signalling. J. Exp. Bot. 2007; 58: 2339–2358. PMID: 17578865

58. Zrenner R, Stitt M, Sonnewald U, Boldt R. Pyrimidine and purine biosynthesis and degradation in plants. Annu. Rev. Plant Biol. 2006; 57: 805–836. PMID: 16669783

59. Stasolla C, Katahira R, Thorpe TA, Ashihara H. Purine and pyrimidine nucleotide metabolism in higher plants. J. Plant Physiol. 2003; 160: 1271–1295. PMID: 14658380

60. Wu Y, Kuzma J, Maréchal E, Graeff R, Lee HC, Foster R. Abscisic acid signaling through cyclic ADP-ribose in plants. Science 1997; 278: 2126–2130. PMID: 9405349

61. Dubovskaya LV, Bakakina YS, Kolesneva EV, Sodel DL, McAinsh MR, Hetherington AM. cGMP-dependent ABA-induced stomatal closure in the ABA-insensitive *Arabidopsis* mutant *abi1-1*. New Phytol. 2011; 191: 57–69. doi: 10.1111/j.1469-8137.2011.03661.x PMID: 21371039

62. Joudoi T, Shichiri Y, Kamizono N, Akaike T, Sawa T, Yoshitake J, et al. Nitrated cyclic GMP modulates guard cell signaling in *Arabidopsis*. Plant Cell 2013; 25: 558–571. doi: 10.1105/tpc.112.105049 PMID: 23396828

63. Kafer C, Zhou L, Santoso D, Guirgis A, Weers B, Park S, et al. Regulation of pyrimidine metabolism in plants. Front. Biosci. 2004; 9: 1611–1625. PMID: 14977572

64. Vogt T. Phenylpropanoid biosynthesis. Mol. Plant 2010; 3, 2–20. doi: 10.1093/mp/ssp106 PMID: 20035037

65. Harris PJ, Hartley RD, Lowry KH. Phenolic constituents of mesophyll and non-mesophyll cell walls from leaf laminae of *Lolium perenne*. J. Sci. Food Agric. 1980; 31: 959–962.

66. Hutzler P, Fischbach R, Heller W, Jungblut TP, Reuber S, Schmitz R, et al. Tissue localization of phenolic compounds in plants by confocal laser scanning microscopy. J. Exp. Bot. 1998; 49: 953–965.

67. Agati G, Azzarello E, Pollastri S, Tattini M. Flavonoids as antioxidants in plants: location and functional significance. Plant Sc. 2012; 196: 67–76.

68. Watkins JM, Hechler PJ, Muday GK. Ethylene-induced flavonol accumulation in guard cells suppresses reactive oxygen species and moderates stomatal aperture. Plant Physiol. 2014; 164: 1707–1717. doi: 10.1104/pp.113.233528 PMID: 24596331

69. Wang SY, Bunce JA, Maas JL. Elevated carbon dioxide increases contents of antioxidant compounds in field-grown strawberries. J. Agric. Food. Chem. 2003; 51: 4315–4320. PMID: 12848504

70. Misra BB, Chen S. Advances in understanding CO_2 responsive plant metabolomes in the era of climate change. Metabolomics 2015. 1–14. doi: 10.1007/s11306-015-0825-4

71. Ziska LH, Panicker S, Wojno HL. Recent and projected increases in atmospheric carbon dioxide and the potential impacts on growth and alkaloid production in wild poppy (*Papaver setigerum* DC.). Clim. Change 2008; 91: 395–403.

72. Ziska LH, Emche SD, Johnson EL, George K, Reed DR, Sicher RC. Alterations in the production and concentration of selected alkaloids as a function of rising atmospheric carbon dioxide and air temperature: implications for ethno-pharmacology. Global Change Biol. 2005; 11: 1798–1807.

73. Qiu QS, Huber JL, Booker FL, Jain V, Leakey AD, Fiscus EL, et al. Increased protein carbonylation in leaves of *Arabidopsis* and soybean in response to elevated [CO_2]. Photosynth. Res. 2008; 97: 155–166. doi: 10.1007/s11120-008-9310-5 PMID: 18506594

74. Gillespie KM, Xu F, Richter KT, McGrath JM, Markelz RC, Ort DR, et al. Greater antioxidant and respiratory metabolism in field-grown soybean exposed to elevated O_3 under both ambient and elevated CO_2. Plant Cell Environ. 2012; 35: 169–184. doi: 10.1111/j.1365-3040.2011.02427.x PMID: 21923758

75. Pérez-López U, Robredo A, Lacuesta M, Sgherri C, Muñoz-Rueda A, Navari- Izzo F, et al. The oxidative stress caused by salinity in two barley cultivars is mitigated by elevated CO_2. Physiol. Plant. 2009; 135: 29–42. doi: 10.1111/j.1399-3054.2008.01174.x PMID: 19121097

76. Foyer CH, Bloom AJ, Queval G, Noctor G. Photorespiratory metabolism: genes, mutants, energetics, and redox signaling. Annu. Rev. Plant Biology 2009; 60: 455–484.

77. Bauwe H, Hagemann M, Fernie AR. Photorespiration: players, partners and origin. Trends Plant Sci. 2010; 15: 330–336. doi: 10.1016/j.tplants.2010.03.006 PMID: 20403720

78. Chen Z, Gallie DR. The ascorbic acid redox state controls guard cell signaling and stomatal movement. Plant Cell 2004; 16: 1143–1162. PMID: 15084716

79. Yi H, Yin J, Liu X, Jing X, Fan S, Zhang H. Sulfur dioxide induced programmed cell death in *Vicia* guard cells. Ecotoxicol. Environ. Saf. 2012; 78: 281–286. doi: 10.1016/j.ecoenv.2011.11.035 PMID: 22154778

80. Wei A, Fu B, Wang Y, Zhai X, Xin X, Zhang C, et al. Involvement of NO and ROS in sulfur dioxide induced guard cells apoptosis in *Tagetes erecta*. Ecotoxicol. Environ. Saf. 2015; 114: 198–203. doi: 10.1016/j.ecoenv.2015.01.024 PMID: 25645141

81. Wei A, Xin X, Wang Y, Zhang C, Cao D. Signal regulation involved in sulfur dioxide-induced guard cell apoptosis in *Hemerocallis fulva*. Ecotoxicol. Environ. Saf. 2013; 98: 41–45. doi: 10.1016/j.ecoenv.2013.09.029 PMID: 24125868

82. Sun Y, Guo H, Yuan L, Wei J, Zhang W, Ge F. Plant stomatal closure improves aphid feeding under elevated CO_2. Global Change Biol. 2015. doi: 10.1111/gcb.12858

83. Zhang S, Li X, Sun Z, Shao S, Hu L, Ye M, et al. Antagonism between phytohormone signaling underlies the variation in disease susceptibility of tomato plants under elevated CO_2. J. Exp. Bot.2015; eru538. doi: 10.1093/jxb/eru538

84. Matros A, Amme S, Kettig B, Buck-Sorlin GH, Sonnewald UWE, Mock HP. Growth at elevated CO_2 concentrations leads to modified profiles of secondary metabolites in tobacco cv. Samsun NN and to increased resistance against infection with potato virus Y. Plant Cell Environ. 2006; 29: 126–137. PMID: 17086759

85. Runion GB, Prior SA, Rogers HH, Mitchell RJ. Effects of elevated atmospheric CO_2 on two southern forest diseases. New Forests 2010; 39: 275–285.

86. Bari R, Jones JD. Role of plant hormones in plant defense responses. Plant Mol. Biol. 2009; 69: 473–488. doi: 10.1007/s11103-008-9435-0 PMID: 19083153

87. Haworth M, Killi D, Materassi A, Raschi A. Coordination of stomatal physiological behavior and morphology with carbon dioxide determines stomatal control. Am. J. Bot. 2015; 102: 677–688. doi: 10.3732/ajb.1400508 PMID: 26022482

88. Price GD, Badger MR, von Caemmerer S. The prospect of using cyanobacterial bicarbonate transporters to improve leaf photosynthesis in C3 crop plants. Plant Physiol. 2011; 155: 20–26. doi: 10.1104/pp.110.164681 PMID: 20923885

89. Yamano T, Sato E, Iguchi H, Fukuda Y, Fukuzawa H. Characterization of cooperative bicarbonate uptake into chloroplast stroma in the green alga *Chlamydomonas reinhardtii*. Proc. Natl. Acad. Sci. U. S. A. 2015;01659.

90. Kamennaya NA, Ahn S, Park H, Bartal R, Sasaki KA, Holman HY, et al. Installing extra bicarbonate transporters in the cyanobacterium *Synechocystis sp*. PCC6803 enhances biomass production. Metab. Eng. 2015; 29: 76–85. doi: 10.1016/j.ymben.2015.03.002 PMID: 25769289

91. Mott KA. Opinion: Stomatal responses to light and CO_2 depend on the mesophyll. Plant Cell Environ. 2009; 32: 1479–1486. doi: 10.1111/j.1365-3040.2009.02022.x PMID: 19627565

92. Araújo WL, Fernie AR, Nunes-Nesi A. Control of stomatal aperture: a renaissance of the old guard. Plant Signal. Behav. 2011; 6: 1305–1311. PMID: 21847028